Quantitative Photothermal Radiometric and FT-IR Photoacoustic Measurements of Specialty Papers

JOSE A. GARCIA,* ANDREAS MANDELIS, MARGARITA MARINOVA, KIRK H. MICHAELIAN, and SHAPOUR AFRASHTEHFAR

Photothermal and Optoelectronic Diagnostics Laboratories, Department of Mechanical and Industrial Engineering and Materials and Manufacturing Ontario, University of Toronto, Toronto, Ontario, Canada M5S 3G8 (J.A.G., A.M., M.M.); Natural Resources Canada, CANMET Western Research Center, 1 Oil Patch Drive, Suite A202 Devon, Alberta, Canada T9G 1A8 (K.H.M.); and Centre Innovation DOMTAR, Domtar Inc., 22025 route Transcanadienne ouest, Sortie 40, Senneville Province Québec, Canada H9X 3L7 (S.A.)

Frequency-domain laser infrared photothermal radiometry (PTR) and photoacoustic Fourier transform spectroscopy (FT-IR/PAS) were used for the measurement of the thermophysical properties (thermal diffusivity, α, and conductivity, *k*) of specialty paper samples with various cotton contents. An improved one-dimensional photothermal model of a free-standing sheet of paper in air that includes both the transmission and backscattering mode was introduced. A high degree of accuracy and reliability was obtained when a multiparameter-fit optimization algorithm was used to examine the transmission and backscattered PTR experimental results. The ability to measure α and its variation, Δα, as a result of the manufacturing process via the PTR technique is invaluable in terms of the quality control of paper products.

Index Headings: **Radiometry; Photothermal; Thermal properties; Papers; Nondestructive tests; Photoacoustic, FT-IR.**

INTRODUCTION

Frequency-domain laser infrared photothermal radiometry (PTR) has been successfully established as a noncontact and nondestructive technique for monitoring the modulated thermal (blackbody) radiation emitted from an optically excited surface of a material after photothermal excitation by a laser.[1,2] The major advantage of PTR over optical methods is its ability to yield reliable measurements of the thermophysical parameters of condensed phases, as well as of the visible and infrared optical absorption/extinction coefficients of organic and optically scattering materials that otherwise may be difficult or impossible to characterize by conventional optical means.[3] As such, it is an excellent candidate for developing a novel nonintrusive characterization/inspection technique for paper and paper products. Furthermore, it has the advantage of relative instrumental, experimental, and interpretational simplicity compared to other noncontact paper characterization techniques, such as laser ultrasonics.[4]

The first thermophysical characterization of commercial paper[5] and counterfeit currency bills[6] by laser PTR was recently reported. A one-dimensional photothermal model of a free-standing sheet of paper in air was presented. However, only the transmission mode of the PTR signal was considered at that time. In this work, both the backscattering and the transmission modes of the PTR signal are investigated experimentally and theoretically. Through a four-parameter fit, the theory is fitted to the data to calculate the thermal diffusivity and thermal conductivity, as well as visible and infrared absorption/extinction coefficients of various specialty paper samples. The reliability of the results of the multiparameter fit is evaluated in terms of sensitivity and uniqueness and further correlated with photoacoustic Fourier transform spectroscopic (FT-IR/PA) analysis of the paper samples.

Received 10 March 1998; accepted 26 May 1998.

* Author to whom correspondence should be sent.

THEORETICAL

The geometry of the theoretical model is shown in Fig. 1. A free-standing sheet (s) of paper of thickness L, thermal diffusivity α_s and thermal conductivity k_s, visible optical absorption/extinction coefficient β_s, and infrared emission coefficient β_{IR} is irradiated with a laser beam of sinusoidally modulated intensity I_0 and angular frequency $\omega = 2\pi f$. The optical constants β_s and β_{IR} are generally unknown combinations of the optical absorption and scattering coefficients at, respectively, the excitation wavelength and the infrared emission wavelength bandwidth collected by the detector optics. According to Kirchhoff's law of detailed balance, the infrared emission constant β_{IR} is equal to the absorption/extinction constant of the sample averaged over the infrared bandwidth of the detector. In the backscattered mode, where the detector is on the same side as the laser-irradiated surface of the sample, the radiometric signal is[7]

$$S_B(\omega) = K\beta_{IR} \int_0^L e^{-\beta_{IR}x} \Delta T_s(x, \omega)\, dx \qquad (1)$$

where K is an instrumental constant depending on geometrical factors, the emissivity averaged over the spectral bandwidth of the detector, and the Stefan–Boltzmann constant. In Eq. 1, $\Delta T_s(x, \omega)$ is the thermal wave field at a depth x in the bulk of the sample.

The determination of $\Delta T_s(x, \omega)$ can be done by considering the thermal-wave system of equations[5]

$$\frac{d^2\Delta T_j(x, \omega)}{dx^2} - \sigma_j^2 \Delta T_j(x, \omega) = 0 \qquad (2)$$

where j = g (gas; air) or s (sample); σ_j is the complex thermal wave number defined as

$$\sigma_j = (1 + i)\sqrt{\frac{\omega}{2\alpha_j}}. \qquad (3)$$

α_j is the thermal diffusivity of material region j. There are three equations involved in Eq. 2, one for each region (g, s, g) in Fig. 1, with solutions in terms of simple ex-

0003-7028/98/5209-1222$2.00/0

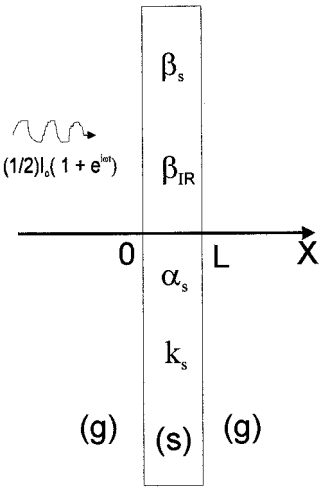

FIG. 1. Schematic diagram of one-dimensional geometry of free-standing paper sheet under laser photothermal excitation and PTR detection. I_0: laser intensity; ω: angular modulation frequency; β_s: visible optical absorption coefficient; β_{IR}: mean infrared absorption coefficient within the spectral bandwith of the MCT detector; α_s: thermal diffusivity of paper; k_s: thermal conductivity of paper; L: paper thickness.

ponential dependencies on the spatial coordinate. For the sample region, the solution takes the form

$$\Delta T_s(x, \omega) = C_1 e^{-\sigma_s x} + C_2 e^{\sigma_s x} - A(\omega) e^{-\beta_s x} \qquad 0 \le x \le L \tag{4}$$

where C_1 and C_2 are integration constants and $A(\omega)$ is the driving term given by

$$A(\omega) = \frac{I_0 \beta_s}{2k_s(\beta_s^2 - \sigma_s^2)}. \tag{5}$$

The integration constants of Eq. 4 can be determined via the boundary conditions of temperature, ΔT_j, and heat flux, $k_j\, \mathrm{d}\Delta T_j/\mathrm{d}x$, continuity at the interfaces 0 and L. Specifically, at the irradiated surface $x = 0$, heat flux conservation of the ac component of the heat transfer equation gives

$$-k_s \frac{\mathrm{d}\Delta T_s}{\mathrm{d}x} + k_g \frac{\mathrm{d}\Delta T_g}{\mathrm{d}x} = \frac{1}{2} I_0. \tag{6}$$

After some algebraic manipulation of Eqs. 4–6, the values of the integration constants C_1 and C_2 are obtained as shown in Eqs. 7 and 8.

$$C_1(\omega) = A(\omega)\left[\frac{(1 - b_{gs})(b_{gs} - r_s)e^{-\beta_s L} + (1 + b_{gs})(b_{gs} + r_s)e^{\sigma_s L}}{(1 + b_{gs})^2 e^{\sigma_s L} - (1 - b_{gs})^2 e^{-\sigma_s L}}\right]. \tag{7}$$

$$C_2(\omega) = A(\omega)\left[\frac{(1 + b_{gs})(b_{gs} - r_s)e^{-\beta_s L} + (1 - b_{gs})(b_{gs} + r_s)e^{-\sigma_s L}}{(1 + b_{gs})^2 e^{\sigma_s L} - (1 - b_{gs})^2 e^{-\sigma_s L}}\right]. \tag{8}$$

In these equations, the following definitions were made:

$$b_{gs} = \frac{k_g \sqrt{\alpha_s}}{k_s \sqrt{\alpha_g}} \qquad r_s \equiv \frac{\beta_s}{\sigma_s}. \tag{9}$$

Finally, upon performing the integration in Eq. 1, using Eqs. 4–9 one obtains the desired expression for the frequency-dependent infrared radiometric backscattering signal, $S_B(\omega)$, as shown in Eq. 10.

$$S_B(\omega) = K\beta_{IR}\left\{C_1\left[\frac{1 - e^{-(\beta_{IR} + \sigma_s)L}}{\beta_{IR} + \sigma_s}\right] + C_2\left[\frac{1 - e^{-(\beta_{IR} - \sigma_s)L}}{\beta_{IR} - \sigma_s}\right] - A(\omega)\left[\frac{1 - e^{-(\beta_{IR} - \beta_s)L}}{\beta_{IR} + \beta_s}\right]\right\}. \tag{10}$$

For detection in the transmission mode, where the detector is on the other side of the laser-irradiated surface of the sample, the radiometric signal is[5,7]

$$S_T(\omega) = K\beta_{IR} \int_0^L e^{-\beta_{IR}(L - x)} \Delta T_s(x, \omega)\, \mathrm{d}x. \tag{11}$$

On following a procedure similar to the one described above, one can obtain the expression for the frequency-dependent infrared radiometric transmission signal as shown in Eq. 12[5]

$$S_T(\omega) = K\beta_{IR}\left\{C_1\left[\frac{e^{-\sigma_s L} - e^{-\beta_{IR} L}}{\beta_{IR} - \sigma_s}\right] + C_2\left[\frac{e^{\sigma_s L} - e^{-\beta_{IR} L}}{\beta_{IR} + \sigma_s}\right] - A(\omega)\left[\frac{e^{-\beta_s L} - e^{-\beta_{IR} L}}{\beta_{IR} - \beta_s}\right]\right\}. \tag{12}$$

EXPERIMENTAL

A schematic diagram of the experimental setup used to perform the PTR measurements of various paper samples is shown in Fig. 2. An intensity-modulated Ar-ion laser (514 nm) from Coherent, Model Innova 100, was used with an expanded pump beam. The spot size was made much larger (8 mm) than the maximum profiling depth ($\sim$ 100 μm) by means of an optical diffuser (a 5 mm thick polymeric substrate with rough surface walls) and aperture to maintain the one-dimensional signal character described by the photothermal-wave theoretical formulation. The intensity of the laser beam was modulated harmonically by using an external sine-wave pulse generator to drive the acousto-optic modulator and to change automatically the modulation frequency applied to it. The working frequency scan was in the 5–1000 Hz range. Signals at frequencies lower than 5 Hz exhibited three-dimensional behavior despite the expanded beam size, owing to the increased lateral (radial) heat diffusion. The laser beam was divided in two by a polarizing beamsplitter. One beam was directed to the backside of the sample for transmission measurements, and the other beam was sent to the front of the sample for backscattered measurements. Only one beam was in use at a time. The emitted IR radiation from the sample was collected and focused onto the detector by using two Ag-coated off-axis paraboloidal mirrors. The detector was a liquid-nitrogen-cooled HgCdTe (MCT) element with an active area of 1 mm^2 and a spectrally selective range of 2–12 μm. A Ge window with a transmission bandwidth of 2–14 μm was mounted in front of the detector to block any visible radiation from the pump laser. The PTR signal from the detector was preamplified (EG&G Judson Mod-

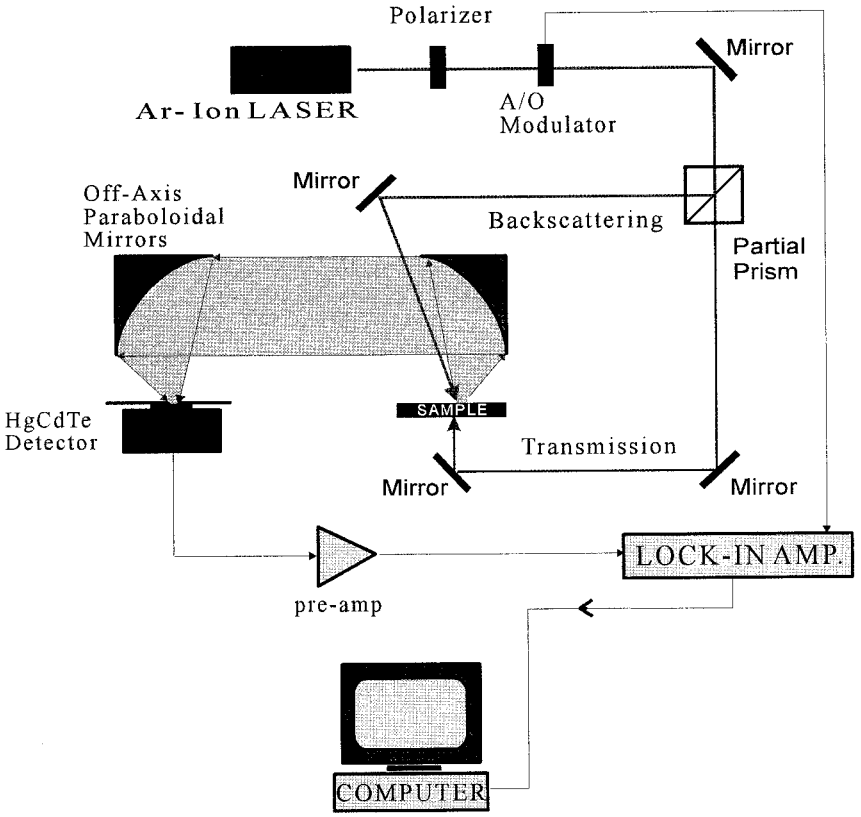

FIG. 2. Experimental setup for infrared PTR of paper.

el PA 350) and fed to a lock-in amplifier (Stanford Research Systems Model SR850). Automatic frequency scans of the acousto-optically modulated laser intensity were controlled by a personal computer. The amplitudes and phases of the PTR signals were stored in the computer for theoretical analysis and calculations.

Photoacoustic (PA) FT-IR spectra of the paper samples were further recorded by using a standard Bruker IFS 88 spectrometer and an MTEC Model 200 gas microphone PA cell. Air was used as the carrier gas in the cell, and the spectrometer was not purged. The interferometer mirror velocity was 0.095 cm/s, giving rise to modulation frequencies between 75 and 750 Hz for the mid-IR region ranging from 400 to 4000 cm^{-1}. The resolution of the FT-IR/PA spectra was 6 cm^{-1}. A PA spectrum of carbon black, obtained under similar conditions, was used to correct the spectra of the papers for the wavelength-dependent spectrometer response.

The PTR and FT-IR/PA results were carefully coordinated so that, for each sample, the same sheet of paper with labeled side orientation was used for both measurements. The FT-IR/PA measurements were obtained by averaging ten 50-scan files (total acquisition time: about 10 min). Each piece of paper was turned over so that the opposite side faced the IR radiation, and a new spectrum was recorded. Owing to the fact that the thickness of the paper (100–135 μm) was much greater than the maximum thermal diffusion length of the FT-IR/PA scan, the data correspond to the side of the paper facing the impinging beam. Therefore, statements about the spectral homogeneity with depth of the various examined paper samples could be made and compared to PTR measurement results.

RESULTS, MULTIPARAMETER FITS, AND DISCUSSION

Laser infrared PTR measurements consisted of frequency scans of various specialty paper samples. Typical PTR responses from backscattering and transmission measurements are shown in Figs. 3 and 4, respectively. This particular sample was paper type S1 made of 100% cotton. Figure 5 shows the FT-IR/PA spectra of both sides of the same sample. When the spectra were superposed and matched at one wavenumber, as shown in that figure, a small degree of inhomogeneity was observed in the relative strength of the peak centered approximately at 1300–1400 cm^{-1}, corresponding to bending vibrations in CH_2 or CH_3 groups.[8]

The theoretical curves superposed on the data of Figs. 3 and 4 were obtained following a computational trial-and-error procedure for optimally fitting simultaneously both the amplitude and the phase of Eq. 10 and Eq. 12 to the experimental data of Fig. 3 and Fig. 4, respectively. In this case, and in other cases where data from the same sample were obtained in both transmission and backscattered modes, each mode was treated independently of the other, in view of the expected depth dependence of parameters, as manifested by the FT-IR/PA spectra. For each mode, it can be seen from Eqs. 10 and 12 that the fits are multivariable involving four fitting parameters: α_s, k_s, β_s, and β_{IR}. No independent measurements of the optical parameters were available for the optical coefficients

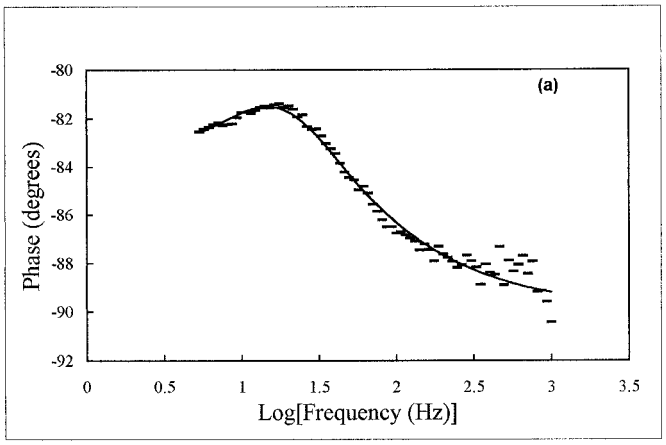

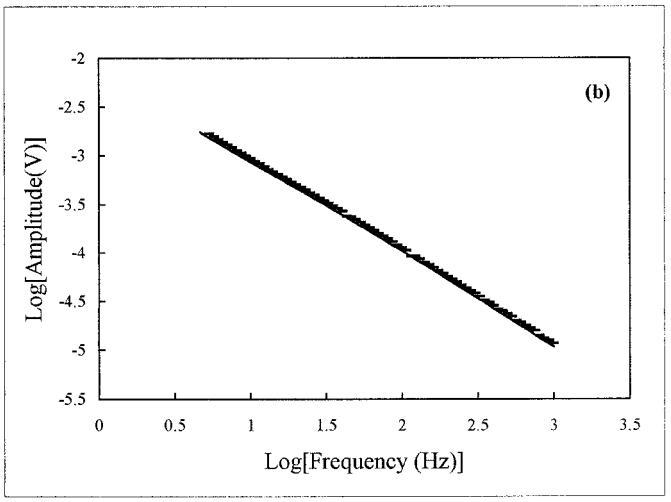

FIG. 3. Experimental PTR backscattered data (– – –) and theoretical multiparameter fits (– – –) to Eq. 10 for sample S1. (**a**) Phase; (**b**) amplitude.

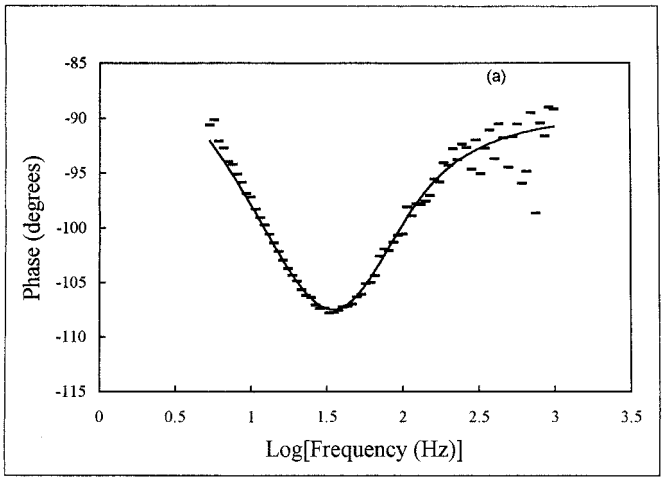

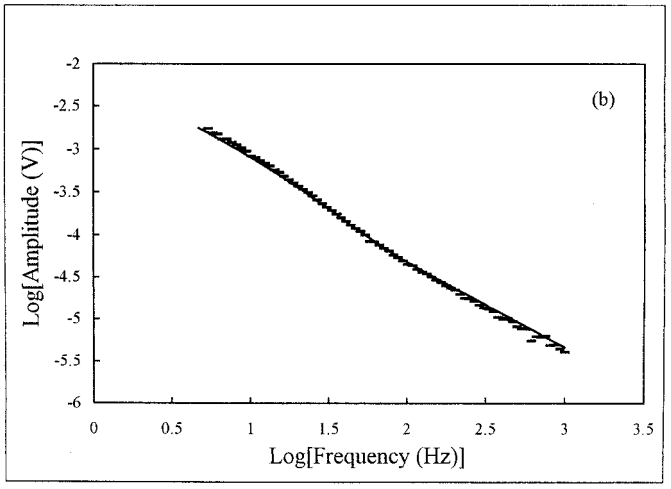

FIG. 4. Experimental PTR transmission data (– – –) and theoretical multiparameter fits (– – –) to Eq. 12 for sample S1. (**a**) Phase; (**b**) amplitude.

β_s and β_{IR}. The simultaneous variation of all four parameters toward a best fit raised the issue of the uniqueness of the fit. In order to address this issue, backscattering and transmission measurements were considered for the same spot on the paper sample. The theory was required to yield acceptable fits to *both* the amplitude and phase data of transmission or backscattering measurements. This procedure raised the level of confidence of the uniqueness of the set of calculated parameters. It was found that the PTR phases are much richer in features than the respective amplitudes and a much better indicator of the sensitivity of the fit to the values of each one of the four fitting parameters. The shape of the phase extrema, backscattered maximum, and transmission minimum (Figs. 3 and 4) depends most sensitively on the value of the thermal diffusivity. These extrema are the result of standing thermal-wave interference pattern equivalents in the bulk of the paper sample, and they depend strongly on the thickness and thermal diffusivity.[9] The width of these extrema depends somewhat more weakly on the thermal conductivity of the paper, which enters the theoretical formalism, Eqs. 2, via the boundary conditions, as opposed to the thermal diffusivity, which is responsible for bulk thermal-wave transport, Eq. 4. It was found that varying these thermophysical parameters to match the transmission phase minimum or backscattered phase maximum could be done without having to consider changes in the optical properties. Therefore, the simultaneous fit of amplitudes and phases was able to produce unique values for the two thermophysical parameters, with the diffusivity being the more sensitive and reliable value by far, on which the actual frequency position of the extremum solely depended. As the primary transport property, the thermal diffusivity values obtained and shown in Table I are considered the most reliable of all the parameter fits. The transmission-generated values represent the thickness-averaged thermal diffusivity, whereas the backscattered-generated values are more readily associated with the near-surface region of the laser-irradiated side. The thermal diffusivity values shown are well within the ranges reported by other investigators using FT-IR photoacoustic spectroscopic detection,[10] visible-laser-radiation photoacoustic gas-cell evaluation,[11] or conventional thermal transport experiments.[12] On the other hand, the reported values of the optical properties (β_s and β_{IR}) are not unique, and a certain degree of cross-compensation was observed, in that deterioration in the goodness of the fit resulting from a decrease in one of

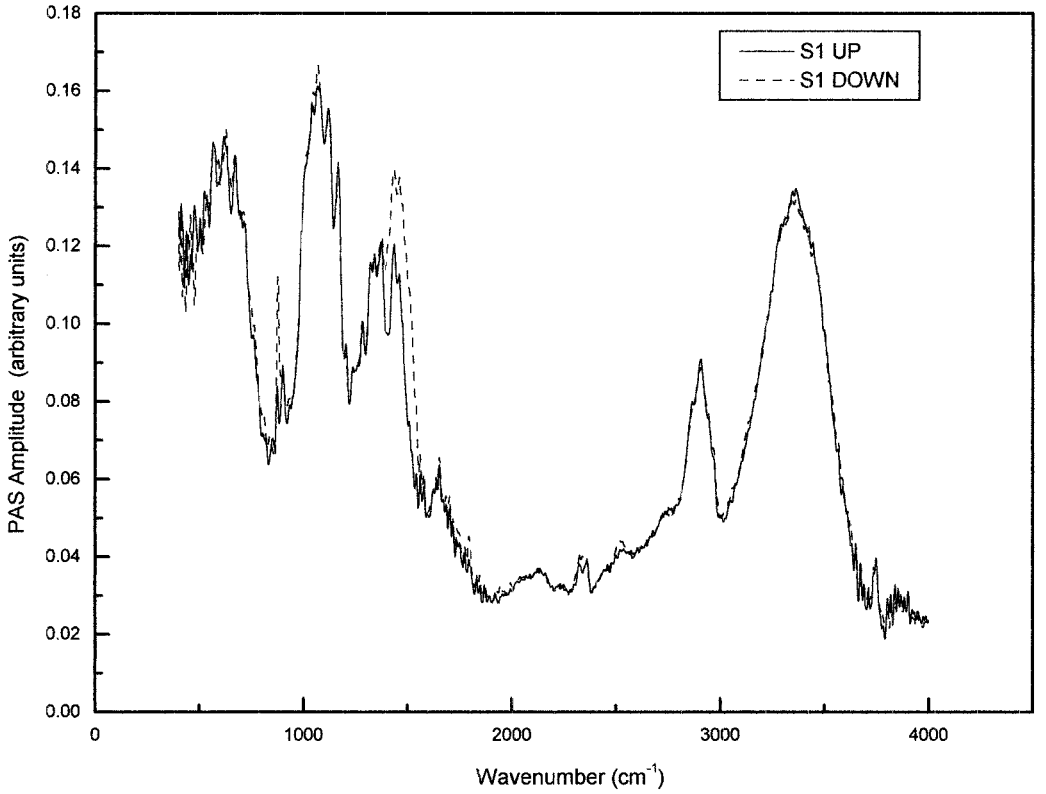

FIG. 5. Amplitude of FT-IR/PA spectra from sample S1 (both surfaces).

these parameters could be restored by compensating (increasing) the value of the other parameter by a similar amount. Independent measurements of at least one of these parameters are thus required to uniquely determine the optical/extinction coefficients of the paper samples. The PTR values of these parameters were thus considered the least reliable measurements in these experiments.

It can be seen from Figs. 3 and 4 that the phases of the particular theoretical fits performed on sample S1 do not exhibit very good agreement at high frequencies, consistent with the FT-IR/PA findings of Fig. 5, which strongly suggest a degree of directional inhomogeneity of this paper (the 1300–1700 cm^{-1} region). This result implies nonconstant depth profiles of either the optical or the thermophysical properties or both. The high-frequency (>100 Hz) regime corresponds to the very near-surface region, the parameters of which can be different from the (assumed uniform) depth-averaged best-fitted values, which were obtained by using the entire frequency range in the computational multiparameter fit. The val-

TABLE I. Measured values of thickness (in mm), thermal diffusivity (α_s), thermal conductivity (k_s), visible absorption coefficient (β_s) and mean infrared optical absorption coefficient (β_{IR}), and instrumental constant (K) of different specialty grades of paper samples of known cotton content and basis weights. Acronyms KP, BFB, and GB refer to the manufacturer trademarks Krypton Parchment, Belfast Bond, and Genoa Bond, respectively. The measurement mode refers to transmission (T) and backscattering (B). Values between parentheses correspond to standard deviation.

Sample	Cotton content (1%)	Basis weight	Manufacturing grade, color	Thickness (μm) (±3)	Measurement mode	α_s ($\times10^{-7}$) ($m^2\ s^{-1}$)	k_s ($W\ m^{-1}\ K^{-1}$)	β_s ($\times10^{-4}$) (m^{-1})	β_{IR} ($\times10^{-4}$) (m^{-1})	K ($\times10^{-4}$)
S1	100	20	KP, Blue White	105	T	1.70	2.21	2.85	2.85	1.81
					B	1.62	2.41	1.80	1.79	2.66
S3	50	20	BFB, White	108	T	1.90	2.00	1.91	1.90	2.10
					B	1.72	3.60	2.41	2.40	4.40
S4	25	20	GB, White	100	T	1.28 (±0.044)	1.00	3.14	3.10	1.21
					B	1.16 (±0.030)	7.00	2.00	2.10	28.0
S5	25	24	C2000, Lumen	135	T	1.60	2.00	2.58	2.57	1.50
					B	1.51	2.50	1.82	1.83	26.0
S6 Front	25	24	GB, White	115	T	1.48	1.51	2.12	2.12	2.65
					B	1.37	2.00	2.47	2.47	4.50
S6 Back	25	24	GB, White	115	T	1.45	1.30	2.89	2.90	2.35
					B	1.30	1.50	1.88	1.89	3.20
S7	100	24	KP, Blue White	126	T	1.62	2.51	2.00	2.00	6.97
					B	1.38	2.50	2.30	2.30	5.63
S8	25	24	C2000, Fluorite	132	T	1.68	1.80	2.65	2.66	5.63
					B	1.58	2.80	2.06	2.05	50.0

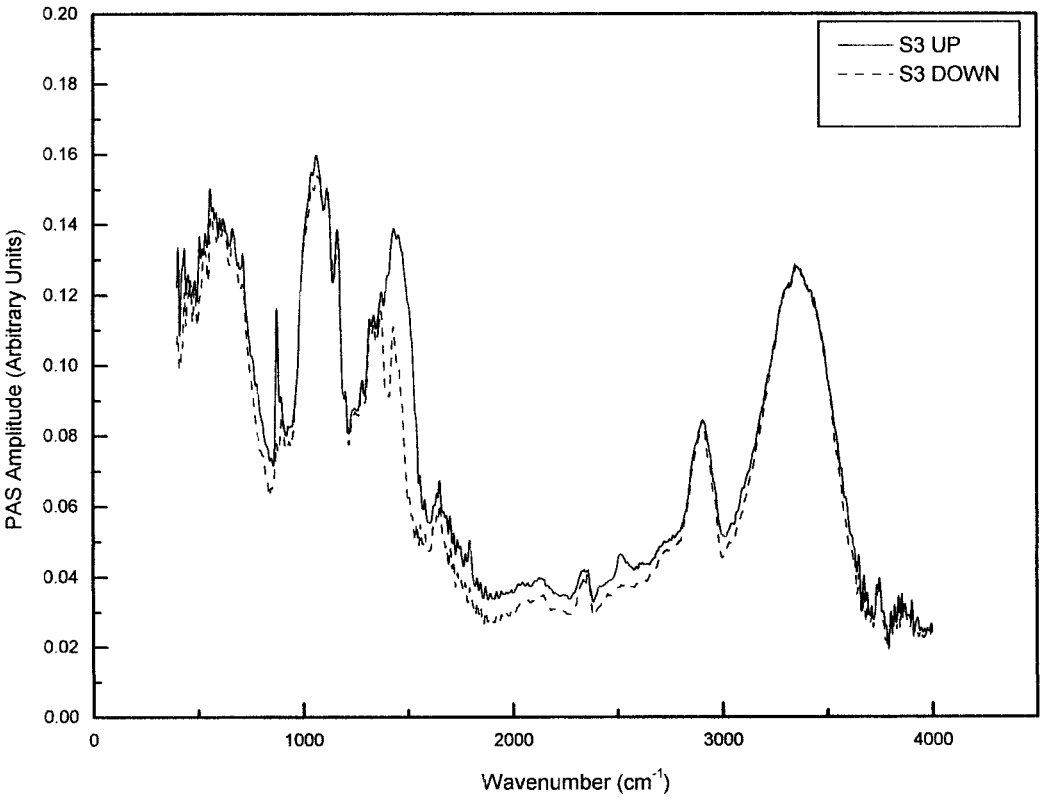

FIG. 6. Amplitude of FT-IR/PA spectra from sample S3 (both surfaces).

ues for the thermophysical and optical parameters obtained from transmission and backscattered measurements for S1 and several other paper samples with various cotton contents and basis weight numbers are shown in Table I. Even though the absolute values of the optical parameters were not found to be reliable, *their order of magnitude* was found to be unique and reliable, in that changes in the reported orders of magnitude ($\sim 10^4$ m^{-1}) made any good fit impossible. Since there appears to be value in these orders of magnitude, which are also consistent with earlier measurements,[5] we decided to report them in Table I. The values of the thermophysical parameters for air used in the calculations were obtained from the literature:[13] $k_g = 2.38 \times 10^{-2}$ W/mK and $\alpha_g = 0.2 \times 10^{-4}$ m^2/s. The thickness of each paper was measured and averaged over five locations on a given sheet. Regarding paper S1, the small degree of inhomogeneity of the FT-IR/PA spectra of both surfaces is accompanied by a relatively small difference in thermal diffusivity and conductivity values. On the other hand, for sample S3, the greater differential in the values of thermal diffusivity and conductivity obtained by transmission and backscattered data is consistent with larger differences between the FT-IR/PA spectra taken from both surfaces, Fig. 6. In this figure it can be seen that the broader spectral range between 1200 and 3200 cm^{-1} has been affected, with the major variations occurring in the 1300–1400 cm^{-1} (CH_2 and CH_3) absorption band. Overall, it appears that the decrease in cotton content from 100 to 50% under the same manufacturing pressure conditions results in higher thermal diffusivity values. This observation may be the result of the decreased mass density ρ of the paper. It should be noted that the thermal diffusivity is related to primary thermophysical properties of a material through the relation

$$\alpha = \frac{k}{\rho C} \tag{13}$$

where C is the specific heat of the material.

Quantitative estimates of the standard deviation of the α_s measurements for paper samples were made by performing several (≥ 3) PTR scans over a large area (several cm^2) of an S4 sheet. The results of the multiparameter fits with regard to thermal diffusivity were averaged and the means and standard deviations were calculated for both transmission and backscattered data, as shown in Table I. It was thus verified that the standard deviations (in parentheses) of the measurements were small (<1–3%), as expected, since the large spot size of the laser beam acted as a signal averager in the lateral (radial) dimension of the sample. A comparison between the samples S4 and S5, both of 25% cotton content but of different origins (GB White vs. C2000 Lumen) and different manufacturing pressures, can be made by considering the ratios of diffusivities from Eq. 13:

$$\frac{\alpha_2}{\alpha_1} = \frac{k_2 \rho_1 C_1}{k_1 \rho_2 C_2}. \tag{14}$$

Assuming that the specific heats are the same for both S4 and S5 samples and that the densities are proportional to the nominal mass density number, data from Table I for S4 (sample "1") and S5 (sample "2") yield a direct ratio of diffusivities equal to 1.21 and a value for the right-hand side of Eq. 14 equal to 1.67. These values represent PTR transmission measurements only and are

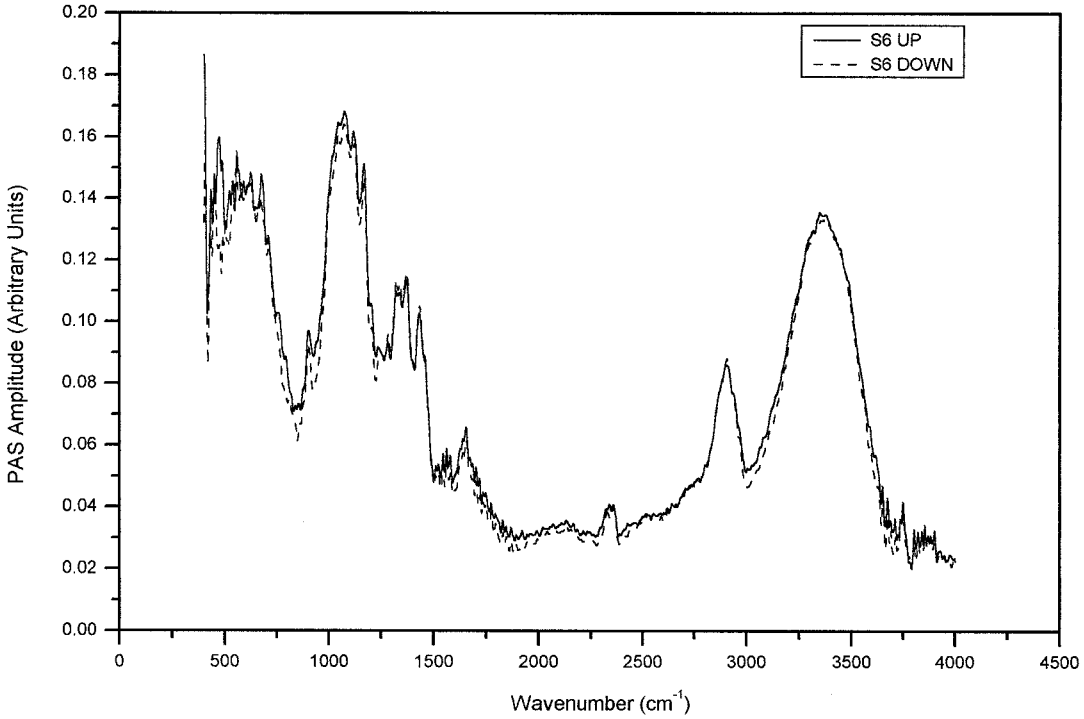

FIG. 7. Amplitude of FT-IR/PA spectra from sample S6 (both surfaces).

quite reasonable in view of the foregoing assumptions. In view of the strong depth inhomogeneity exhibited by sample S4, calculations based on backscattered PTR data were considered unreliable for quantitative conclusions. Sample S6 was measured from both sides by using PTR transmission and backscattering modes. The two transmission α_s values were found to be within 2% of each other, as expected from thickness-averaged measurements. In contrast to sample S4, however, this paper exhibited nearly symmetric near-surface behavior with close values (to within 5%) of the thermal diffusivities measured from backscattered data. The high degree of two-sided near-surface homogeneity of this sample is further corroborated by the very similar FT-IR/PA spectra of both sides shown in Fig. 7. It should be recalled that FT-IR/PA spectroscopy yields near-surface spectra of each side of paper samples.

The much larger differences in α_s between transmission and backscattered data of the sample S7 shown in Table I are accompanied by similar differences in the 1300–2500 cm^{-1} region of the FT-IR/PA spectra taken from both surfaces. Those spectral differences are similar to the ones observed in the case of sample S3 (Fig. 6) and are not shown here. It is interesting to compare sample S7 to sample S1, which are very similar except for different manufacturing mass density values. The thickness-averaged transmission value of S7 is somewhat lower than that of S1, in agreement with the ρ^{-1} dependence of α_s (Eq. 13). The difference $\Delta\alpha = \alpha_T - \alpha_B$ is, however, much greater for S7 than for S1, corroborating evidence from the FT-IR/PA spectra of these two samples, according to which the extent of spectral differences between the two sides of S7 is much greater than that of S1 (Fig. 5), rather resembling the situation with sample S3, which also exhibits large $\Delta\alpha$. Quantitative estimates of the origin of the diffusivity variations between samples S1 and S7 can be given by using Eq. 14 and Table I under the assumption of equal specific heats. This is a much better assumption between these two samples than between S4 and S5, in view of their similar manufacturing conditions. The direct ratio of diffusivities of S1 over S7 in transmission is 1.05. The right-hand side of Eq. 14 gives a value of 1.056, in excellent agreement. Similarly, the relevant backscattered measurement values are 1.17 and 1.16. It can be concluded that the remarkable similarities in α support the common manufacturing origin of S1 and S7, whereas the equally remarkable differences in their $\Delta\alpha$ are indicative of the extent of depth inhomogeneities during their manufacture.

Finally, a comparison between samples S5 and S8, which are identical in manufacture except for the color of the paper, points to some other possibilities for depth inhomogeneity. The transmission and backscattering values of diffusivity of both samples are quite close to each other, as expected, with $\Delta\alpha \sim 0.1 \times 10^{-7}$ m^2/s. The FT-IR/PA spectra of both samples exhibit differences in peak heights throughout the entire spectrum. Figure 8 represents sample S8. The absorption band centered in the 1050 cm^{-1} region is most likely associated with the C–O single-bond stretching vibration in cellulose.[8,14,15] The band centered in the 2900 cm^{-1} region represents C–H stretching.[8,15] The broad band around 3300 cm^{-1} arises from hydrogen-bonded OH groups (O–H stretching),[8,15] presumably in water. Differences in peak intensity are indicative of different concentrations of compounds between the two surfaces of S8 (and similarly of S5), possibly due to local variation in concentration of components or even different surface conditions, roughness, and atmospheric moisture absorption. To understand the possible origins of all the observed inhomogeneities, more

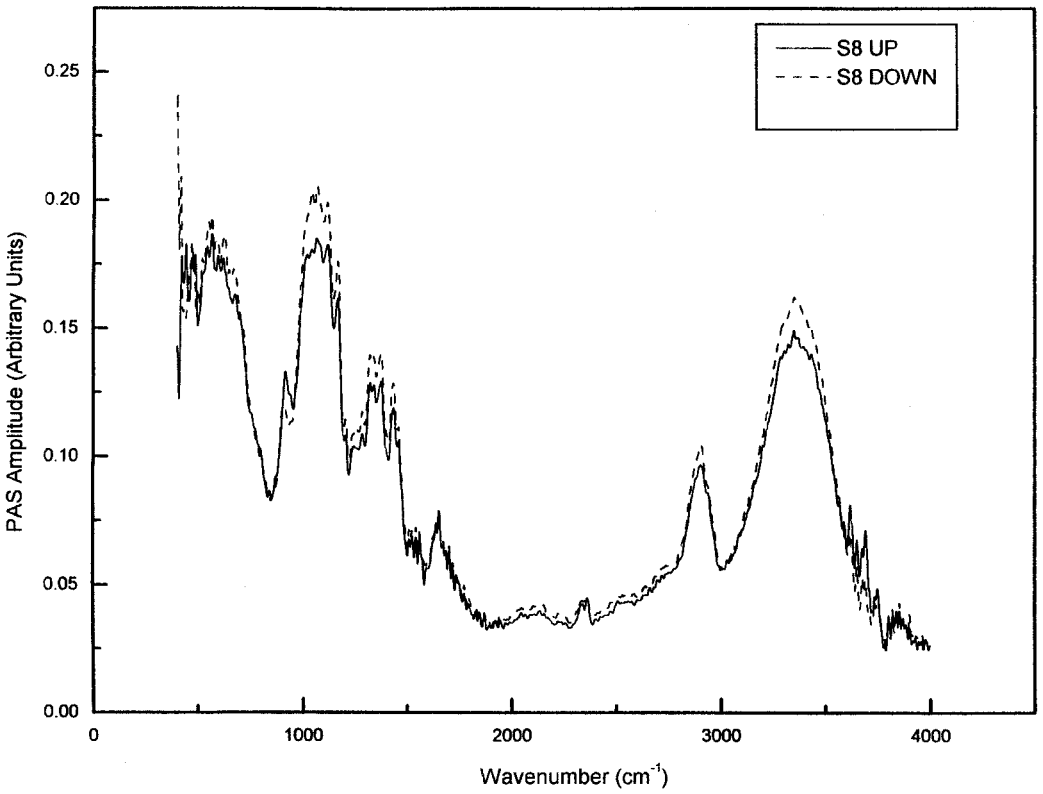

FIG. 8. Amplitude of FT-IR/PA spectra from sample S8 (both surfaces).

combined PTR and FT-IR/PA studies of highly controlled paper samples will be required.

CONCLUSION

In this combined PTR and FT-IR/PA study, theoretical and experimental methodologies were established for the measurement of the thermophysical properties (thermal diffusivity and conductivity) to a higher degree of accuracy and reliability than is evident in earlier work,[5] owing to an improved multiparameter-fit optimization algorithm and the combination of transmission and backscattered PTR data. The FT-IR/PA spectra from several samples corroborated the variations in values of thermal diffusivity, the primary and most reliable parameter, and indicated depth-dependent structural inhomogeneities in the specialty paper samples to a larger (samples S4, S7; $\Delta\alpha \sim 0.2 \times 10^{-7}$ m^2/s) or a smaller (sample S6; $\Delta\alpha \sim 0.07 \times 10^{-7}$ m^2/s) extent. For samples of similar manufacturing origin, such as S1 and S7, the measured values of diffusivity were found to depend on both mass density and thermal conductivity. The calculations support the hypothesis that the specific heat varies little with manufacturing pressure; the density is proportional to the nominal manufacturing mass density value, and the variations in the values of thermal conductivity measured via the PTR technique are consistent with the definition in Eq. 13. Further studies of controlled paper samples via the FT-IR/PA spectroscopic technique may improve our understanding of the chemical origin(s) of the depth inhomogeneities. Irrespective of its interpretation, the ability to measure α and $\Delta\alpha$ via the PTR technique is invaluable with respect to quality control of the paper manufacturing process.

ACKNOWLEDGMENTS

The support of the Manufacturing Research Corporation of Ontario (MRCO), presently Materials and Manufacturing Ontario (MMO), is gratefully acknowledged. Paper samples were kindly supplied by Domtar, Inc.

1. R. D. Tom, E. P. O'Hara, and D. Benin, J. App. Phys. **53,** 5392 (1982).
2. A. Mandelis, M. Munidasa, and A. Othonos, IEEE J. Quant. Electron. **29,** 1948 (1993).
3. A. Rosencwaig, *Photoacoustics and Photoacoustic Spectroscopy,* (John Wiley and Sons, New York, 1980).
4. Y. H. Berthelot and M. A. Johnson, Opt. Eng. **36,** 408 (1997).
5. A. Mandelis, M. Nestoros, A. Othonos, and C. Christofides, J. Pulp Paper Sci. **23,** J108 (1997).
6. A. Othonos, A. Mandelis, M. Nestoros, and C. Christofides, Opt. Eng. **36,** 400 (1997).
7. W. P. Leung and A. C. Tam, J. App. Phys. **56,** 153 (1984).
8. M.-L. Kuo, J. F. McClelland, S. Luo, P.-L. Chien, R. D. Walker, and C.-Y. Hse, Wood Fiber Sci. **20,** 132 (1988).
9. J. Shen, and A. Mandelis, Rev. Sci. Instrum. **66,** 4999 (1995).
10. J. R. Harbour, M. A. Hopper, R. H. Marchessault, C. J. Dobbin, and E. Anczurowski, J. Pulp Paper Sci. **11,** J42 (1985).
11. J. P. Jaarinen, R. Y. Rajala, T. P. Tiusanen, and M. Luukkala, IEEE Trans. Sonics Ultrasonics **SU-32,** 375 (1985).
12. D. J. Sanders and R. C. Forsyth, Rev. Sci. Instrum. **54,** 238 (1984).
13. *CRC Handbook of Chemistry and Physics,* D. R. Lide, Ed. (Chemical Rubber Company, Cleveland, Ohio, 1993), 74th ed., pp. 6-1 and 6–199.
14. K. Krishnan, Appl. Spectrosc. **35,** 549 (1981).
15. N. Gurnagul, F. G. T. St-Germain, and D. G. Gray, J. Pulp Paper Sci. **12,** J156 (1986).